

Article

Magnetic Micro Sensors with Two Magnetic Field Effect Transistors Fabricated Using the Commercial Complementary Metal Oxide Semiconductor Process

Wei-Ren Chen ¹, Yao-Chuan Tsai ², Po-Jen Shih ³, Cheng-Chih Hsu ⁴ and Ching-Liang Dai ^{1,*}

¹ Department of Mechanical Engineering, National Chung Hsing University, Taichung 402, Taiwan; wei-then@hotmail.com

² Department of Bio-Industrial Mechatronics Engineering, National Chung Hsing University, Taichung 402, Taiwan; yctsaii@dragon.nchu.edu.tw

³ Department of Biomedical Engineering, National Taiwan University, Taipei 106, Taiwan; pjshih@ntu.edu.tw

⁴ Department of Electro-Optical Engineering, National United University, Miaoli 360, Taiwan; cchsu920624@nuu.edu.tw

* Correspondence: cldai@dragon.nchu.edu.tw; Tel.: +886-4-22840433

Received: 15 July 2020; Accepted: 19 August 2020; Published: 21 August 2020



Abstract: The fabrication and characterization of a magnetic micro sensor (MMS) with two magnetic field effect transistors (MAGFETs) based on the commercial complementary metal oxide semiconductor (CMOS) process are investigated. The magnetic micro sensor is a three-axis sensing type. The structure of the magnetic microsensor is composed of an x/y-MAGFET and a z-MAGFET. The x/y-MAGFET is employed to sense the magnetic field (MF) in the *x*- and *y*-axis, and the z-MAGFET is used to detect the MF in the *z*-axis. To increase the sensitivity of the magnetic microsensor, gates are introduced into the two MAGFETs. The sensing current of the MAGFET enhances when a bias voltage is applied to the gates. The finite element method software Sentaurus TCAD was used to analyze the MMS's performance. Experiments show that the MMS has a sensitivity of 182 mV/T in the *x*-axis MF and a sensitivity of 180 mV/T in the *y*-axis MF. The sensitivity of the MMS is 27.8 mV/T in the *z*-axis MF.

Keywords: magnetic microsensor; magnetic field effect transistor; CMOS; MEMS

1. Introduction

Magnetic micro sensors (MMS) play an important role in measurement of magnetic field and are applied in various fields. For instance, Mohri [1] employed amorphous wire complementary metal oxide semiconductor (CMOS) integrated circuit (IC) magnetoimpedance to design a magnetic micro sensor, and the sensor was applied in the electric compass of smartphones and the magnetic guidance self-driving system. A respiratory training and monitoring system for radiotherapy, presented by Oh [2], was developed using a microelectromechanical system (MEMS) magnetic micro sensor (MMS). This system was composed of an MEMS MMS, a small magnet and a breathing output component. Sideris [3] has proposed a 2×2 MMS fabricated using the CMOS technology. The MMS array was applied in bio-detection assays. A three-axis MEMS MMS, fabricated by Li [4], was a digital tunneling magnetoresistance type. The MMS with a CMOS interface circuit has been used in the field of nanosatellites. Vetrella [5] has used an MEMS MMS to design a cooperative unmanned aerial vehicle navigation system. The system includes an MMS, an inertial sensor, a global positioning system receiver, a vision component, and a navigation algorithm to stabilize and control the flight of an unmanned aerial vehicle. A tunnel magnetoresistance MMS, designed by Tavassolizadeh [6], has been applied in sensing micro- and nano-scale strain. The experiments showed that the tunnel magnetoresistance MMS has an ability to measure both compressive and tensile stresses. Gooneratne [7] has made a

micro-chip consisting of a magnetoresistive MMS and a unique magnetic actuator. The micro-chip can integrate with microfluidic components and electronic circuitry for biomolecule quantification detection. Zhang [8] has used a three-axis MMS to measure the steel condition in reinforced concrete bridges. Jogschies [9] has introduced a magnetoresistive MMS manufactured on a flexible substrate. The flexible MMS has been applied to the flexible write head of data storage components.

In addition to the manufacture of integrated circuits, the standard CMOS process is also used to produce various micro sensors [10–13] and microactuators [14,15]. Many MMSs have also been developed using the standard CMOS process. For example, Li [16] developed an MMS with a conducting magnetic structure using a CMOS process. The MMS was bonded on a printed circuit board. The sensor became more sensitive due to the conducting magnetic structure located above the MMS. The MMS sensitivity was 132 mV/T. Oh [17] used a CMOS process to design a vertical-type Hall MMS with a four-contact structure. Compared with Oh's previous MMS [17], the sensitivity of the sensor increased by 13 times because of the vertical-type design and four-contact structure. A three-axis MMS, presented by Lin [18], was made using CMOS technology. The MMS consisted of four Hall elements and a magnetotransistor. The four Hall elements detected the magnetic field (MF) in z -axis. The magnetotransistor measured the magnetic field in the x/y -axis. The MMS had a sensitivity of 0.69 V/T in the x -axis MF and a sensitivity of 0.55 V/T in the y -axis MF. The sensitivity of the MMS exceeded that of Li [16]. Osberger [19] presented an MMS fabricated using a standard CMOS process. A chopper-stabilized magnetic field effect transistor was employed to design the MMS and to enhance the sensing resolution of the MMS. A three-axis MMS, proposed by Tseng [20], was made using a standard CMOS process. The MMS was a magnetotransistor that included eight collectors, four bases, and a ring emitter. Amplifier circuitry integrated with the MMS magnified the voltage output of the MMS. The experimental results showed that the MMS had a sensitivity of 6.5 mV/T in the x -axis MF and a sensitivity of 6.5 mV/T in the y -axis MF. The sensitivity of the MMS was lower than that of Li [16] and Lin [18]. A fluxgate MMS, which was presented by Lu [21], was produced using CMOS-MEMS technology. The fluxgate MMS was bounded on a printed circuit board using a flip-chip packaging method, and the printed circuit board had planar pick-up coils, three-dimensional excitation coils, and dual magnetic cores. The maximum responsivity of the fluxgate MMS was 593 V/T at the excitation frequency of 50 kHz. The minimum MF noise of the fluxgate MMS was 0.05 nT/ $\sqrt{\text{Hz}}$. The fluxgate MMS required a post-CMOS process; thus, the fabrication of the fluxgate was more complicated than that of Li [16], Oh [17], Lin [18], Osberger [19], and Tseng [20]. A three-axis MMS, developed by Leepattarapongpan [22], was made using a CMOS process. The MMS was a magnetotransistor, its structure including four collectors, four bases, and one emitter. The MMS sensitivity was 14.5%/T in the range 0–400 mT. Sung [23] fabricated an MMS using a CMOS process. The MMS was a folded vertical Hall element. The MMS used a lateral folded structure and a guard ring to reduce the cross-coupling noise. Kimura [24] developed a two-dimensional MMS using a standard CMOS process. The MMS consisted of a 64×64 array of the Hall element, and it had a low-frequency noise of 16%. Jiang [25] utilized a standard CMOS process to make an MMS. The MMS that combined spinning-current Hall elements and pick-up coils had a resolution of 210 μT in a bandwidth of 3 MHz. A two-dimensional MMS, proposed by Kimura [26], was made based on the CMOS technology. The MMS was a 16×16 array of the Hall element, and the average sensitivity of the MMS was 0.140 mV/mT. The sensitivity of MMS approached that of Li [16] but was smaller than that of Lin [18].

These magnetic micro sensors [16–19,21,23,25,26] fabricated by CMOS technology were 1-axis MF sensors. The MMS developed by Lin [18] was a three-axis sensor, but its cross-sensitivity was high because the structure of the MMS had only one magnetotransistor. Therefore, this work develops a three-axis MMS fabricated by the commercial CMOS process. To avoid the cross-coupling effect and reduce the cross-sensitivity, the MMS was composed of two magnetic field effect transistors (MAGFETs): an x/y -MAGFET and a z -MAGFET. The x/y -MAGFET measured the MF in the x - and y -axis, and the z -MAGFET measured the MF in the z -axis.

2. Structure of the MMS

The magnetic micro sensor is composed of an x/y-MAGFET and a z-MAGFET. The x/y-MAGFET detects the MF in the x - and y -axis. The z-MAGFET senses the MF in the z -axis. Figure 1a illustrates the structure of the x/y-MAGFET, where B1, B2, B3, and B4 are the bases of the x/y-MAGFET; C1, C2, C3, and C4 are the collectors of the x/y-MAGFET; G1, G2, G3, and G4 are the gates of the x/y-MAGFET; and E is the emitter of the x/y-MAGFET. The x/y-MAGFET uses shallow trench isolation (STI) oxide to limit the current movement direction and to reduce the leakage current.

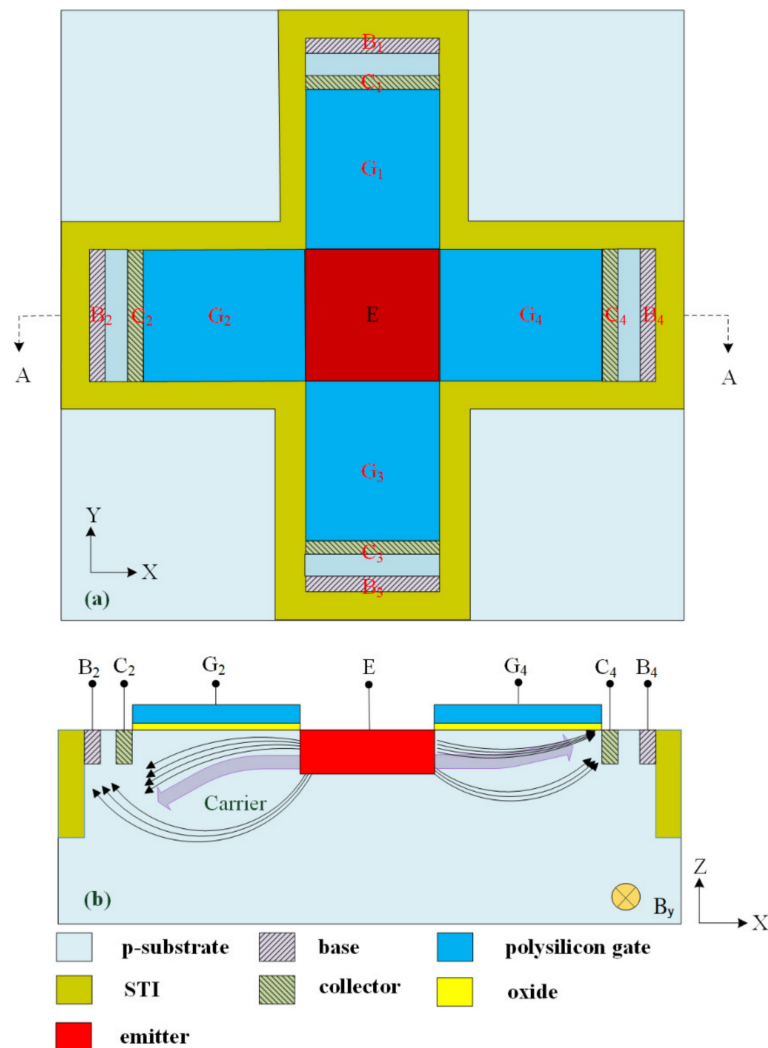


Figure 1. (a) Structure of the x/y magnetic field effect transistor (MAGFET); (b) Cross-sectional view of the x/y-MAGFET along line AA.

Figure 1b illustrates a cross-sectional view of the x/y-MAGFET along line AA. When a bias voltage is applied to the gates of the x/y-MAGFET, the surface of the p-substrate forms a channel under the gate, increasing the mobility of carriers and enhancing the sensitivity of the MMS. The sensing principle of the x/y-MAGFET is as follows. Carriers move from the emitter to the bases and collectors through applying the bias voltages to the bases, collectors, and gates. Because the Lorentz force acts, carriers on the right in Figure 1b are deflected upward when an MF in the y -axis applies to the x/y-MAGFET. A small number of carriers move to the base B₄ owing to the collector C₄ obstructing their movement paths. Most carriers move to the collector C₄, resulting in the current of the collector C₄ increasing. On the other hand, because the Lorentz force acts, carriers on the left in Figure 1b are deflected downward when an MF in the y -axis applies to the x/y-MAGFET. Most carriers pass

across the collector C_2 and move to the base B_2 , resulting in the current of the collector C_2 decreasing. Thereby, the x/y -MAGFET has a voltage difference between the collectors C_2 and C_4 in the y -axis MF. The voltage difference of the collectors C_2/C_4 is the output voltage (OV) of the MMS in the y -axis MF.

Similarly, carriers move from the emitter to the bases and collectors through applying the bias voltages to the bases, collectors, and gates. Because the Lorentz force acts, carriers moving to the collector C_1 are deflected downward when an MF in the x -axis is applied to the x/y -MAGFET. Most carriers pass across the collector C_1 and move to the base B_1 , resulting in the current of the collector C_1 decreasing. Additionally, because the Lorentz force acts, carriers moving to the collector C_3 are deflected upward when an MF in the x -axis is applied to the x/y -MAGFET. A small number of carriers move to the base B_3 owing to the collector C_3 obstructing their movement paths. Most carriers move to the collector C_3 , increasing the current of the collector C_3 . Thereby, the x/y -MAGFET has a voltage difference between the collectors C_1 and C_3 in the x -axis MF. The voltage difference of the collectors C_1/C_3 is the MMS OV in the y -axis MF.

Figure 2 illustrates the structure of the z -MAGFET, where B_{1z} , B_{2z} , B_{3z} , and B_{4z} are the bases of the z -MAGFET; G_{1z} , G_{2z} , G_{3z} , and G_{4z} are the gates of the z -MAGFET; E_z is the emitter of the z -MAGFET; and C_{1z} , C_{2z} , C_{3z} , C_{4z} , C_{5z} , C_{6z} , C_{7z} , and C_{8z} are the collectors of the z -MAGFET. The STI oxide limits the current movement direction and reduces the leakage current for the z -MAGFET. Carriers move from the emitter to the bases and collectors when bias voltages are applied to the gates, collectors, and bases. Because of the Lorentz force acting, carriers are deflected toward the collectors C_{2z} , C_{4z} , C_{6z} , and C_{8z} when an MF in the z -axis is applied to the z -MAGFET. The current produces an imbalance between the collectors C_{1z} and C_{2z} , resulting in the z -MAGFET having a voltage difference with the collectors C_{1z}/C_{2z} in the z -axis MF. Similarly, the collectors between the electrodes C_{3z}/C_{4z} , C_{5z}/C_{6z} , and C_{7z}/C_{8z} , respectively, produce a voltage difference in the z -axis MF. All voltage differences in the series are the MMS OV in the z -axis MF.

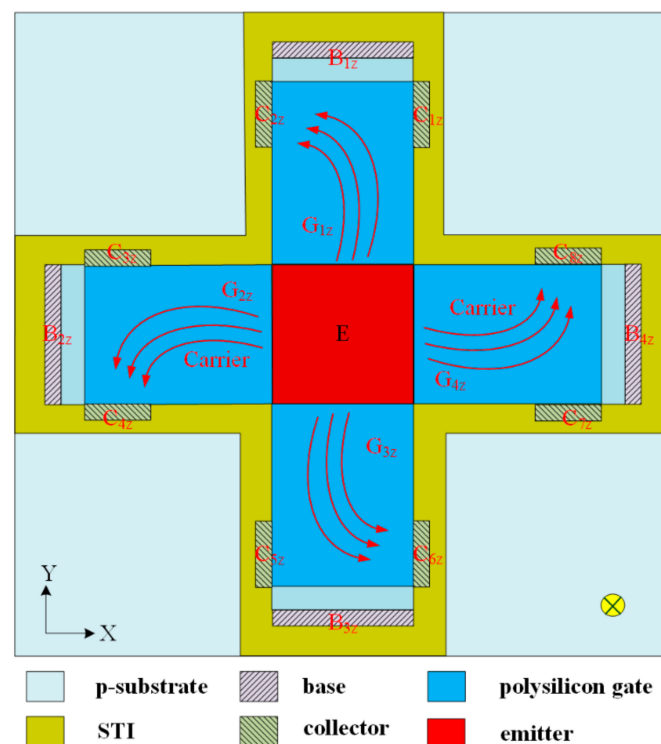


Figure 2. Structure of the z -MAGFET.

The finite element method software Sentaurus TCAD was used to analyze the MMS characteristic. A model of the x/y -MAGFET (Figure 1a) was established, and the model was meshed using the Delaunay triangulation approach. The electrical and MF coupling effect for the x/y MAGFET was

analyzed using the Poisson electron hole method. The carrier density distribution of the x/y -MAGFET was solved using the Bank–Rose method. Figure 3 shows the simulated OV for the MMS in the x -axis MF. In the simulation, the voltage of the bases and collectors for the x/y -MAGFET was 3.3 V. The bases and collectors connected with a resistance of 1 k Ω , respectively. The voltage of the gates for the x/y -MAGFET was 0.4 V. An MF in the x -axis was provided to the x/y -MAGFET. The simulated results showed that the MMS OV in the x -axis MF changed from -35 mV at -200 mT to 35 mV at 200 mT. The x/y -MAGFET was a symmetrical structure, so the MMS characteristic in the y -axis MF was the same as that in the x -axis MF. Thereby, the simulated OV of the MMS in the y -axis MF was the same as that of the MMS in the x -axis MF.

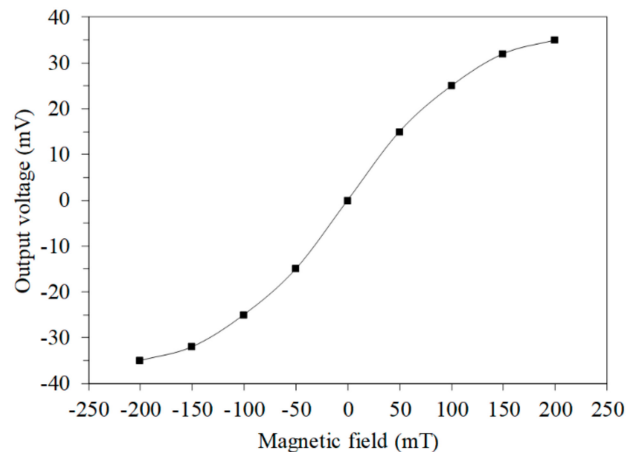


Figure 3. Simulated output voltage (OV) in the y -axis magnetic field.

With the same simulation method, the MMS OV in the z -axis MF was simulated. The model of the z -MAGFET (Figure 2) was established, and the OV of the z -MAGFET in the z -axis MF was simulated. Figure 4 shows the MMS OV in the z -axis MF. In the simulation, the voltage of the gates for the z -MAGFET was 0.4 V. The bases and collectors connected with a resistance of 1 k Ω , respectively. The voltage of the bases and collectors for the z -MAGFET was 3.3 V. The z -axis MF was applied to the z -MAGFET. The results showed that the simulated OV of the MMS in the z -axis MF varied from -6.5 mV at -200 mT to 6.5 mV at 200 mT.

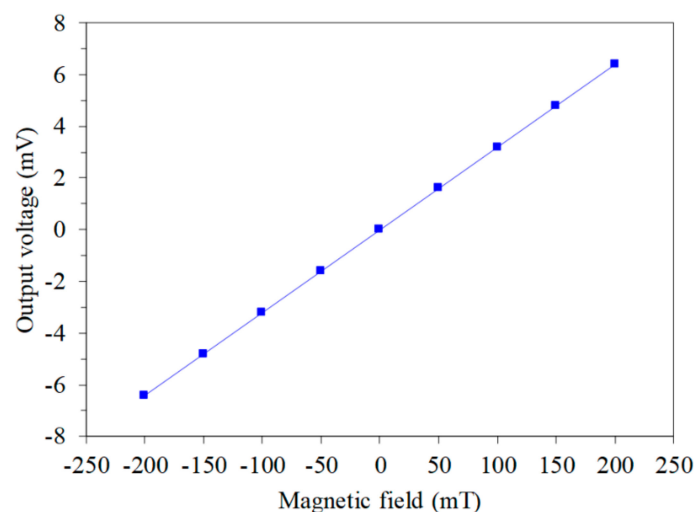


Figure 4. Simulated OV in the z -axis magnetic field.

3. Fabrication of the MMS

The magnetic micro sensor consisted of an x/y -MAGFET and a z -MAGFET. Figure 1 shows the structure of the x/y -MAGFET, and Figure 2 shows the structure of the z -MAGFET. The layout of the

x/y-MAGFET was designed according to the structure in Figure 1. At the same time, the layout of the z-MAGFET was designed in accordance with the structure in Figure 2. The MMS was manufactured utilizing the commercial CMOS process [27–29]. According to the layout of the MMS, the Taiwan Semiconductor Manufacturing Company (TSMC) made the MMS based on the commercial 0.18 μm CMOS process. Figure 5 demonstrates an optical image of the MMS after completion of the CMOS process. As shown in Figure 5, the MMS chip has a z-MAGFET and an x/y-MAGFET. To measure the characteristic of the MMS chip, the MMS chip was wire-bonded on a printed circuit board. Figure 6 shows a picture of the MMS after wire-bonding.

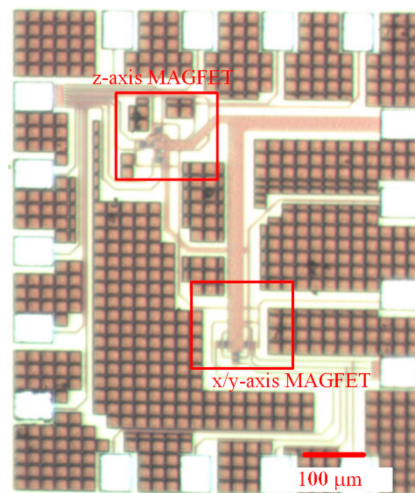


Figure 5. Optical image of the magnetic micro sensor (MMS) chip.

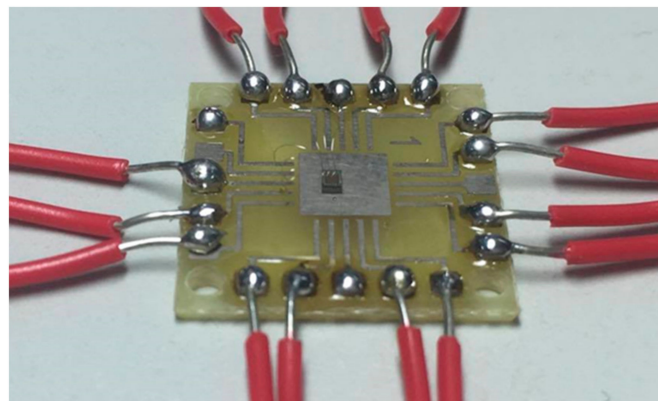


Figure 6. Picture of the MMS after wire-bonding.

4. Results

Figure 7 shows the experimental setup of the MMS. A Gauss meter, a digital multimeter, a magnetic field generator (MFG), and two power supplies were employed to measure the MMS characteristic. The MMS was set in the MFG. One power supply provided power to the MFG, and the other one provided power to the MMS. The MFG produced an MF to the MMS. The magnitude of the MF generated by the MFG was calibrated using the Gauss meter. The MMS OV was recorded using the digital multimeter.

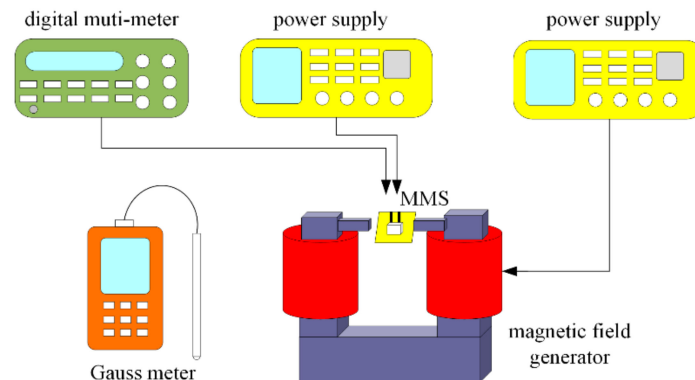


Figure 7. Experimental setup for the MMS.

First, the characteristic of the MMS in the x -axis MF was measured. As shown in Figure 7, the MMS was set in the MFG, and the MFG provided an MF range of -200 to 200 mT to the x/y -MAGFET. The bases and collectors of the x/y -MAGFET were applied with a bias voltage of 3.3 V. The gates of the x/y -MAGFET were applied with different voltages. The bases and collectors connected with a resistance of 1 k Ω . The digital multimeter recorded the voltage difference of the collectors C_2/C_4 for the x/y -MAGFET. Figure 8 shows the tested OV for the MMS in the x -axis MF, where V_G is the gate voltage of the MAGFET. When $V_G = 0$ V, the MMS OV changed from -28 mV at -200 mT to 27.2 mV at 200 mT. When $V_G = 0.2$ V, the MMS OV varied from -29 mV at -200 mT to 30.3 mV at 200 mT. The MMS was more sensitive to the MF at $V_G = 0.4$ V, and its OV increased from -32.5 mV at -200 mT to 31.8 mV at 200 mT. The curves in Figure 8 are nonlinear. The least squares method was employed to analyze the linear regression of the curves. The analysis showed that the slope of the regression line at $V_G = 0.4$ V was 182 mV/T. The sensitivity of the MMS in the x -axis MF was 182 mV/T.

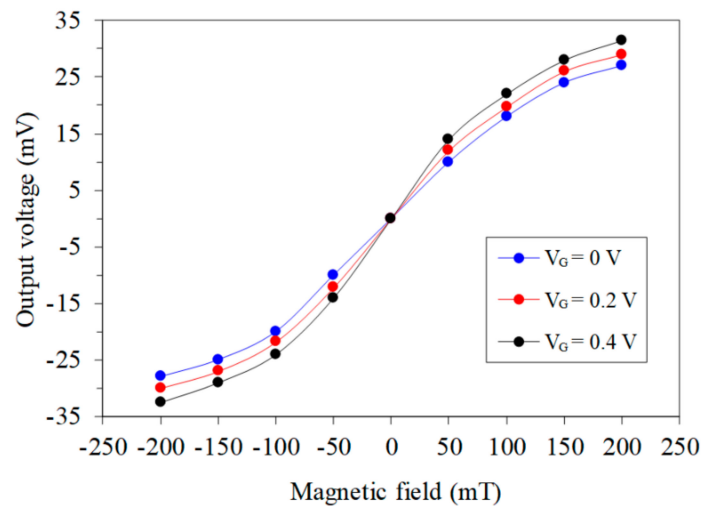


Figure 8. Tested OV in the x -axis magnetic field.

The characteristic of the MMS in the y -axis MF was tested. The MFG generated a y -axis MF and applied it to the x/y -MAGFET. The power supply provided a bias voltage of 3.3 V to the bases and collectors of the x/y -MAGFET. The gates of the x/y -MAGFET were applied with different voltages. The bases and collectors connected with a resistance of 1 k Ω . The voltage difference of the collectors C_1/C_3 for the x/y -MAGFET was measured using the digital multimeter. Figure 9 shows the tested OV for the MMS in the y -axis MF, where V_G is the gate voltage of the MAGFET. When $V_G = 0$ V, the sensitivity of the MMS was the lowest and its OV varied from -27.6 mV at -200 mT to 26.8 mV at 200 mT. When $V_G = 0.2$ V, the MMS OV changed from -29.5 mV at -200 mT to 28.7 mV at 200 mT. When $V_G = 0.4$ V, the MMS was more sensitive to the MF and its OV increased from -32.2 mV at

−200 mT to 31.4 mV at 200 mT. The least squares method was utilized to evaluate the linear regression of the curves in Figure 9. The results showed that the slope of the regression line at $V_G = 0.4$ V was 180 mV/T. The sensitivity of the MMS in the y -axis MF was 180 mV/T.

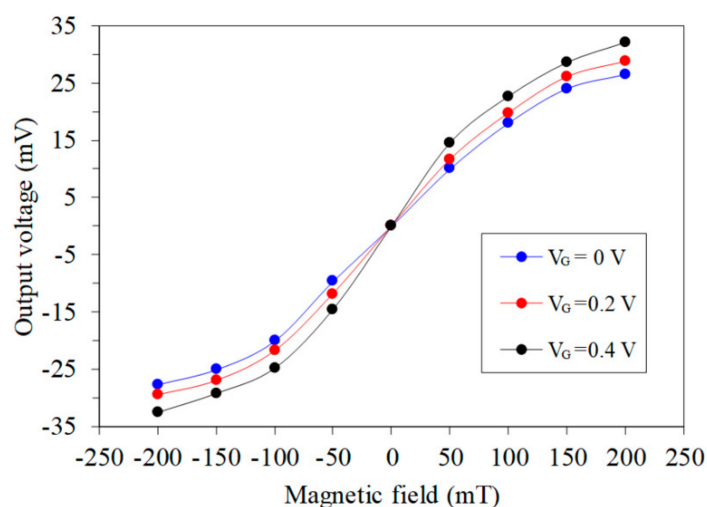


Figure 9. Tested OV in the y -axis magnetic field.

The characteristic of the MMS in the z -axis MF was tested. A z -axis MF, which was produced by the MFG, was applied to the z -MAGFET. A bias voltage of 3.3 V was applied to the bases and collectors of the z -MAGFET. The gates of the z -MAGFET were applied with different voltages. The bases and collectors connected with a resistance of 1 k Ω . The digital multimeter was used to test the OV of the z -MAGFET. Figure 10 shows the tested OV for the MMS in the z -axis MF, where V_G is the gate voltage of the MAGFET. The MMS was insensitive to the MF at $V_G = 0$ V. As the gate voltage increased, the MMS OV became strong. When $V_G = 0.2$ V, the MMS OV changed from −3.6 mV at −200 mT to 3.7 mV at 200 mT. When $V_G = 0.4$ V, the MMS OV increased from −5.6 mV at −200 mT to 5.8 mV at 200 mT. The slope of the curve at $V_G = 0.4$ V was 27.8 mV/T. Therefore, the sensitivity of the MMS in the z -axis MF was 27.8 mV/T. When the Lorentz force acts, the number of carriers (z -MAGFET in Figure 2) deflected to the side is smaller than the number of carriers (x/y -MAGFET in Figure 1) that are deflected upward or downward. Therefore, the output voltage and sensitivity of the z -MAGFET are smaller than that of the x/y -MAGFET.

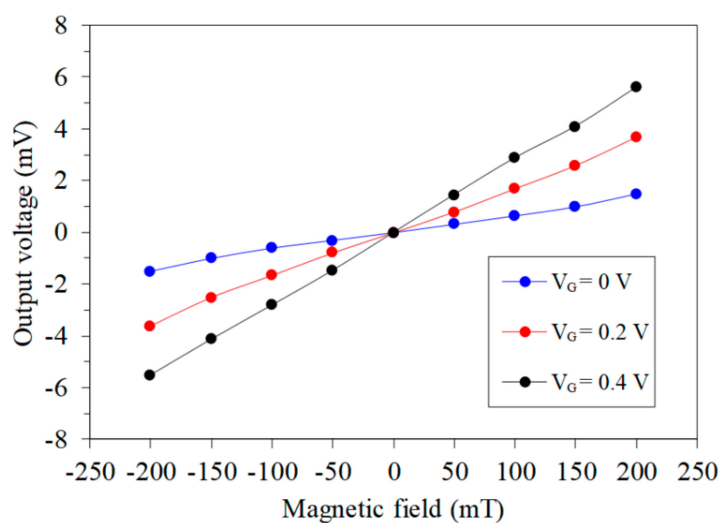


Figure 10. Tested OV in the z -axis magnetic field.

To understand the cross-sensitivity of the MMS, the OV for each axis of the MMS was measured in the same MF. First, an MF in the x -axis was applied to the MMS. The bases and collectors of the x/y -MAGFET and z -MAGFET were applied with a bias voltage of 3.3 V. A gate voltage of 0.4 V was applied to the gates of the x/y -MAGFET and z -MAGFET. The OVs of the x/y -MAGFET and z -MAGFET were measured using the digital multimeter. Figure 11 shows the OV for each axis of the MMS in the x -axis MF, where $V_o(x,x)$ is the x -direction OV of the x/y -MAGFET in the x -axis MF; $V_o(x,y)$ is the y -direction OV of the x/y -MAGFET in the x -axis MF; and $V_o(x,z)$ is the OV of the z -MAGFET in the x -axis MF. As shown in Figure 11, the $V_o(x,y)$ and $V_o(x,z)$ are low in the x -axis MF. The slope of the curve $V_o(x,y)$ was 8.2 mV/T, and the slope of the curve $V_o(x,z)$ was 3.4 mV/T. Thereby, the MMS had a cross-sensitivity of 8.2 mV/T (y -direction output) and a cross-sensitivity of 3.4 mV/T (z -direction output) in the x -axis MF. The sensitivity of the MMS in the x -axis MF was 182 mV/T. Compared to the sensitivity of the MMS, the cross-sensitivity of the MMS in x -axis MF was less than 6%.

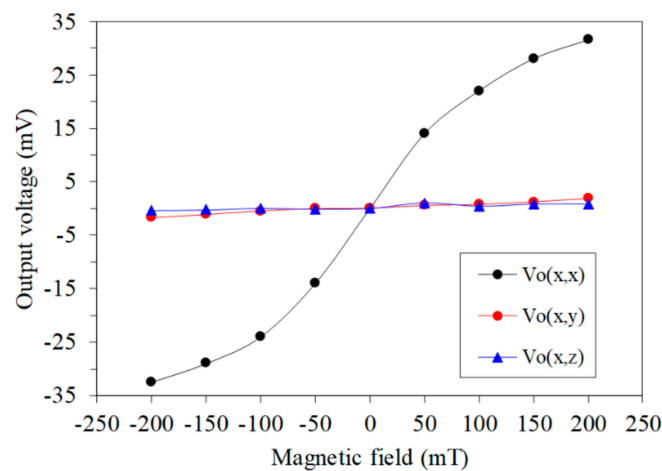


Figure 11. Output of the MMS in the x -axis magnetic field.

A magnetic field in the y -axis was applied to the MMS. A bias voltage of 3.3 V was applied to the bases and collectors of the x/y -MAGFET and z -MAGFET. The gate voltage of the x/y -MAGFET and z -MAGFET was 0.4 V. The digital multimeter recorded the OV of the x/y -MAGFET and z -MAGFET. Figure 12 shows the OV for each axis of the MMS in the y -axis MF, where $V_o(y,x)$ is the x -direction OV of the x/y -MAGFET in the y -axis MF; $V_o(y,y)$ is the y -direction OV of the x/y -MAGFET in the y -axis MF; and $V_o(y,z)$ is the OV of the z -MAGFET in the y -axis MF. As shown in Figure 12, the $V_o(y,x)$ and $V_o(y,z)$ are low in the y -axis MF. The slope of the curve $V_o(y,x)$ was 7.8 mV/T, and the slope of the curve $V_o(y,z)$ was 3.2 mV/T. Thereby, the MMS had a cross-sensitivity of 7.8 mV/T (x -direction output) and a cross-sensitivity of 3.2 mV/T (z -direction output) in the y -axis MF. The sensitivity of the MMS in the y -axis MF was 180 mV/T. Compared to the sensitivity of the MMS, the cross-sensitivity of the MMS in y -axis MF was less than 6%.

The z -axis MF was applied to the MMS. The gate voltage of the x/y -MAGFET and z -MAGFET was 0.4 V. The bases and collectors of the x/y -MAGFET and z -MAGFET were applied with a bias voltage of 3.3 V. The OV of the x/y -MAGFET and z -MAGFET was recorded using the digital multimeter. Figure 13 shows the OV for each axis of the MMS in the z -axis MF, where $V_o(z,x)$ is the x -direction OV of the x/y -MAGFET in the z -axis MF; $V_o(z,y)$ is the y -direction OV of the x/y -MAGFET in the z -axis MF; and $V_o(z,z)$ is the OV of the z -MAGFET in the z -axis MF. As shown in Figure 13, the $V_o(z,x)$ and $V_o(z,y)$ are low in the z -axis MF. The slope of the curve $V_o(z,x)$ was 1.3 mV/T, and the slope of the curve $V_o(z,y)$ was 1.1 mV/T. Thereby, the MMS had a cross-sensitivity of 1.3 mV/T (x -direction output) and a cross-sensitivity of 1.1 mV/T (y -direction output) in the z -axis MF. The sensitivity of the MMS in the z -axis MF was 27.8 mV/T. Compared to the sensitivity of the MMS, the cross-sensitivity of the MMS in z -axis MF was less than 6%.

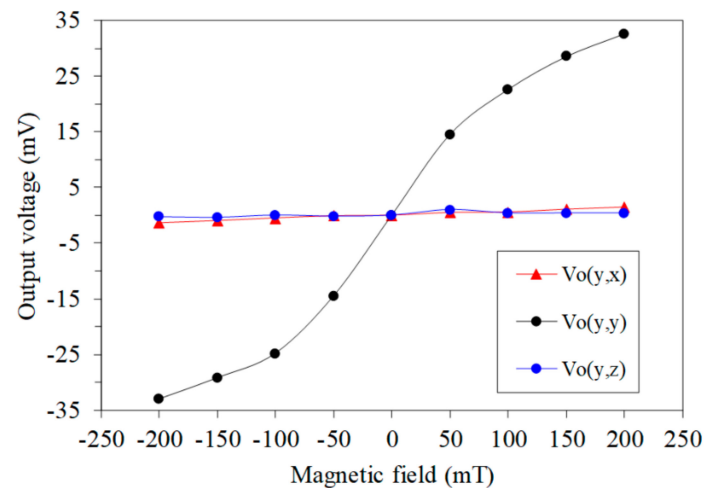


Figure 12. Output of the MMS in the y -axis magnetic field.

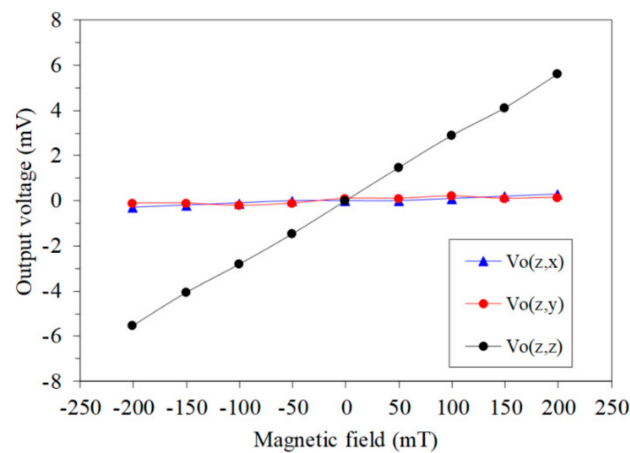


Figure 13. Output of the MMS in the z -axis magnetic field.

Table 1 lists the sensitivities for various MMS manufactured using CMOS. The MMS developed by Li [16], Xu [30], and Zhao [31] were 1-axis MF sensors, and the MMS presented by Yang [32] was a 2-axis MF sensor. As shown in Table 1, the sensitivity of the MMS in this work in the x - and y -axis MF exceeded that of Li [16], Tseng [20], and Kimura [26]. The sensitivity of the MMS presented by Tseng [20] in the z -axis MF was lower than that of this work.

Table 1. Sensitivity for various MMS.

| MMS | Sensitivity (mV/T) | | |
|-------------|--------------------|-----------|-----------|
| | x -axis | y -axis | z -axis |
| Li [16] | 132 | | |
| Lin [18] | 690 | 530 | 91 |
| Tseng [20] | 6.5 | 6.5 | 0.4 |
| Kimura [26] | 140 | | |
| Xu [30] | | | 31 |
| Yang [32] | 366 | 365 | |
| Zhao [31] | | | 264 |
| This work | 182 | 180 | 27.8 |

5. Conclusions

A three-axis magnetic micro sensor with an x/y -MAGFET and a z -MAGFET was manufactured using the commercial $0.18 \mu\text{m}$ CMOS process. The x/y -MAGFET was used to sense the MF in the x - and

y-axis, and the *z*-MAGFET was utilized to detect the MF in the *z*-axis. The gates of the *x/y*-MAGFET and the *z*-MAGFET increased the mobility of carriers in the surface of the *p*-substrate and enhanced the sensitivity of the MMS. The MMS was fabricated without a post-CMOS process. The fluxgate MMS presented by Lu [21] needed a post-CMOS process. Fabrication of the MMS was simpler than that of the fluxgate MMS [21]. The experiments showed that the MMS had a sensitivity of 182 mV/T in the *x*-axis MF and a sensitivity of 180 mV/T in the *y*-axis MF. The sensitivity of the MMS was 27.8 mV/T in the *z*-axis MF. The finite element method software, Sentaurus TCAD, was employed to simulate the output voltage of the MMS. The simulated output voltage of the MMS was in agreement with the measured output voltage of the MMS. According to the experimental results, the cross-sensitivity of the MMS in *x*- and *y*-axis MF was less than 6%. The cross-sensitivity of the MMS in *z*-axis MF was also less than 6%. Therefore, the MMS had a high sensitivity and a low cross-sensitivity.

Author Contributions: Conceptualization, C.-L.D.; Data curation, P.-J.S.; Formal analysis, W.-R.C.; Funding acquisition, C.-L.D. and Y.-C.T.; Investigation, W.-R.C., Y.-C.T. and C.-L.D.; Methodology, Y.-C.T. and C.-L.D.; Project administration, C.-L.D.; Resources, C.-C.H.; Software, W.-R.C. and P.-J.S.; Supervision, C.-L.D.; Validation, P.-J.S. and C.-C.H.; Writing—original draft, W.-R.C.; Writing—review & editing, C.-L.D. All authors have read and agreed to the published version of the manuscript.

Funding: This research received an external funding from the Ministry of Science and Technology (MOST) of the Republic of China with Contract No. MOST 108-2221-E-005-065-MY2.

Acknowledgments: The authors would like to thank the Ministry of Science and Technology (MOST) of the Republic of China for financially supporting this research under Contract No. MOST 108-2221-E-005-065-MY2.

Conflicts of Interest: The authors declare no conflict of interest.

References

1. Mohri, K.; Yamamoto, M.; Uchiyama, T. Application topics of amorphous wire CMOS IC magneto-impedance micromagnetic sensors for I-o-T smart society. *J. Sens.* **2019**, *2019*, 8285240. [[CrossRef](#)]
2. Oh, Y.; Jung, Y.J.; Choi, S.H.; Kim, D.W. Design and evaluation of a MEMS magnetic field sensor-based respiratory monitoring and training System for radiotherapy. *Sensors* **2018**, *9*, 2742. [[CrossRef](#)]
3. Sideris, C.; Khial, P.P.; Hajimiri, A. Design and implementation of reference-free drift-cancelling CMOS magnetic sensors for biosensing applications. *IEEE J. Solid State Circuits* **2018**, *53*, 3065–3075. [[CrossRef](#)]
4. Li, X.Y.; Hu, J.P.; Chen, W.P.; Yin, L.; Liu, X.W. A novel high-precision digital tunneling magnetic resistance-type sensor for the nanosatellites' space application. *Micromachines* **2018**, *9*, 121. [[CrossRef](#)] [[PubMed](#)]
5. Vetrella, A.R.; Fasano, G.; Accardo, D.; Moccia, A. Differential GNSS and vision-based tracking to improve navigation performance in cooperative multi-UAV systems. *Sensors* **2016**, *16*, 2164. [[CrossRef](#)] [[PubMed](#)]
6. Tavassolizadeh, A.; Rott, K.; Meier, T.; Quandt, E.; Holscher, H.; Reiss, G.; Meyners, D. Tunnel magneto-resistance sensors with magnetostrictive electrodes: Strain sensors. *Sensors* **2016**, *16*, 1902. [[CrossRef](#)] [[PubMed](#)]
7. Gooneratne, C.P.; Kodzius, R.; Li, F.Q.; Foulds, I.G.; Kosel, J. On-chip magnetic bead manipulation and detection using a magnetoresistive sensor-based micro-chip: Design considerations and experimental characterization. *Sensors* **2016**, *16*, 1369. [[CrossRef](#)] [[PubMed](#)]
8. Zhang, H.; Liao, L.; Zhao, R.Q.; Zhou, J.T.; Yang, M.; Xia, R.C. The non-destructive test of steel corrosion in reinforced concrete bridges using a micro-magnetic sensor. *Sensors* **2016**, *16*, 1439. [[CrossRef](#)]
9. Jogschies, L.; Klaas, D.; Kruppe, R.; Rittinger, J.; Taptimthong, P.; Wienecke, A.; Rissing, L.; Wurz, M.C. Recent developments of magnetoresistive sensors for industrial applications. *Sensors* **2015**, *15*, 28665–28689. [[CrossRef](#)]
10. Yang, M.Z.; Dai, C.L.; Shih, P.J. An acetone microsensor with a ring oscillator circuit fabricated using the commercial 0.18 μm CMOS process. *Sensors* **2014**, *14*, 12735–12747. [[CrossRef](#)]
11. Dai, C.L.; Chen, Y.C.; Wu, C.C.; Kuo, C.F. Cobalt oxide nanosheet and CNT micro carbon monoxide sensor integrated with readout circuit on chip. *Sensors* **2010**, *10*, 1753–1764. [[CrossRef](#)] [[PubMed](#)]
12. Yang, M.Z.; Dai, C.L.; Wu, C.C. Sol-Gel zinc oxide humidity sensors integrated with a ring oscillator circuit on-a-chip. *Sensors* **2014**, *14*, 20360–20371. [[CrossRef](#)] [[PubMed](#)]

13. Dai, C.L.; Kao, P.H.; Tai, Y.W.; Wu, C.C. Micro FET pressure sensor manufactured using CMOS-MEMS technique. *Microelectron. J.* **2008**, *39*, 744–749. [[CrossRef](#)]
14. Lin, C.Y.; Hsu, C.C.; Dai, C.L. Fabrication of micromachined capacitive switch using the CMOS-MEMS technology. *Micromachines* **2015**, *6*, 1645–1654. [[CrossRef](#)]
15. Cheng, Y.C.; Dai, C.L.; Lee, C.Y.; Chen, P.H.; Chang, P.Z. A circular micromirror array fabricated by a maskless post-CMOS process. *Microsyst. Technol.* **2005**, *11*, 444–451. [[CrossRef](#)]
16. Li, X.L.; Zhao, X.F.; Wen, D.Z. Characteristics of a magnetic field sensor with a concentrating-conducting magnetic flux structure. *Sensors* **2019**, *19*, 4498. [[CrossRef](#)]
17. Oh, S.; Hwang, D.Y.; Chae, H. 4-Contact structure of vertical-type CMOS Hall device for 3-D magnetic sensor. *IEICE Electron. Expr.* **2019**, *16*, 20180854. [[CrossRef](#)]
18. Lin, Y.N.; Dai, C.L. Micro magnetic field sensors manufactured using a standard 0.18- μm CMOS process. *Micromachines* **2018**, *9*, 393. [[CrossRef](#)]
19. Osberger, L.; Frick, V. Analysis, design, and optimization of the CHOPFET magnetic field transducer. *IEEE Trans. Electron Dev.* **2018**, *65*, 3454–3459. [[CrossRef](#)]
20. Tseng, J.Z.; Shih, P.J.; Hsu, C.C.; Dai, C.L. A three-axis magnetic field microsensors fabricated utilizing a CMOS process. *Appl. Sci.* **2017**, *7*, 1289. [[CrossRef](#)]
21. Lu, C.C.; Huang, J.; Chiu, P.K.; Chiu, S.L.; Jeng, J.T. High-Sensitivity low-noise miniature fluxgate magnetometers using a flip chip conceptual design. *Sensors* **2014**, *14*, 13815–13829. [[CrossRef](#)] [[PubMed](#)]
22. Leepattarapongpan, C.; Phetchakul, T.; Penpondee, N.; Pengpad, P.; Srihapat, A.; Jeathsaksiri, W.; Chaowicharat, E.; Hruanun, C.; Poyai, A. A merged magnetotransistor for 3-axis magnetic field measurement based on carrier recombination-deflection effect. *Microelectron. J.* **2014**, *45*, 565–573. [[CrossRef](#)]
23. Sung, G.M.; Yu, C.P. 2-D differential folded vertical Hall device fabricated on a p-type substrate using CMOS technology. *IEEE Sens. J.* **2013**, *13*, 2253–2262. [[CrossRef](#)]
24. Kimura, T.; Sakairi, Y.; Mori, A.; Masuzawa, T. Suppression method of low-frequency noise for two-dimensional integrated magnetic sensor. *Jpn. J. Appl. Phys.* **2017**, *56*, 04CF05. [[CrossRef](#)]
25. Jiang, J.F.; Makinwa, K.A.A. Multipath wide-bandwidth CMOS magnetic sensors. *IEEE J. Solid State Circuits* **2017**, *52*, 198–209. [[CrossRef](#)]
26. Kimura, T.; Uno, K.; Masuzawa, T. Size-Reduced two-dimensional integrated magnetic sensor fabricated in 0.18- μm CMOS process. *IEEJ Trans. Electr. Electron. Eng.* **2015**, *10*, 345–349. [[CrossRef](#)]
27. Yang, M.Z.; Wu, C.C.; Dai, C.L.; Tsai, W.J. Energy harvesting thermoelectric generators manufactured using the complementary metal oxide semiconductor process. *Sensors* **2013**, *13*, 2359–2367. [[CrossRef](#)]
28. Dai, C.L.; Chiou, J.H.; Lu, M.S.C. A maskless post-CMOS bulk micromachining process and its application. *J. Micromech. Microeng.* **2005**, *15*, 2366–2371. [[CrossRef](#)]
29. Yang, M.Z.; Dai, C.L. Ethanol microsensors with a readout circuit manufactured using the CMOS-MEMS technique. *Sensors* **2015**, *15*, 1623–1634. [[CrossRef](#)]
30. Xu, Y.; Pan, H.B.; He, S.Z.; Li, L. A highly sensitive CMOS digital Hall sensor for low magnetic field applications. *Sensors* **2012**, *12*, 2162–2174. [[CrossRef](#)]
31. Zhao, X.F.; Wen, D.Z.; Zhuang, C.C.; Liu, G.; Wang, Z.Q. High sensitivity magnetic field sensors based on nano-polysilicon thin-film transistors. *Chinese Phys. Lett.* **2012**, *29*, 118501. [[CrossRef](#)]
32. Yang, X.; Zhao, X.; Bai, Y.; Lv, M.; Wen, D. Two-dimensional magnetic field sensor based on silicon magnetic sensitive transistors with differential structure. *Micromachines* **2017**, *8*, 95. [[CrossRef](#)]

